JOURNAL OF THEORETICAL
AND APPLIED MECHANICS
https://doi.org/10.15632/jtam-pl/204360
ONLINE FIRST

FRICTIONLESS EDGE SUPPORT FOR THREE-POINT BENDING TESTS IN THE NONLINEAR REGION

Péter MÁTÉ*, András SZEKRÉNYES

Department of Applied Mechanics, Faculty of Mechanical Engineering,
Budapest University of Technology and Economics, Budapest, Hungary
*corresponding author, *peter.mate@mm.bme.hu*

In this article, a newly developed support type is presented for three-point bending in the nonlinear region. The support can keep the contact point's location static during the loading process, thus imitating an edge-like support with theoretically no radius and friction. The support can be used for measurements in the region of large deflections without having to consider the displacement of the contact point or dissipative forces. The support was tested on fiber reinforced composite and steel beams. During the measurements, the movement of the supports and the beam shape was monitored using digital image processing.

Keywords: three-point bending; large deflection; digital image processing; material testing.

1. Introduction

Three-point bending tests are widely used in the industry for easy and relatively cheap material testing. They are reliable and are less demanding than proper tensile tests in terms of instrumentation. Three-point bending tests feature loads usually only in the linear region, where the rotation of the beam at the supports is negligible. Thus, the linearized solution for the beam deflection holds true. If one exceeds these boundaries and increases the beam deflection to the point where the specimen starts slipping on the supports, the solution used for the test evaluation cannot be applied, because the reaction forces are not parallel anymore (Arnautov, 2005; Batista, 2015; Mujika, 2006; West, 1964).

For bending tests in the nonlinear region, the supports are usually cylindrical and running on bearings to decrease the frictional forces (Batista, 2015; Mujika, 2006; West, 1964). Although it makes friction negligible, it induces new nonlinearities into the system. As the deflection increases, the contact point of the rollers and the beam changes location, as shown in Fig. 1a (Arnautov, 2005; Batista, 2015; Máté & Szekrényes, 2020). Using simple edges as a support to fix the contact point (as presented in Fig. 1b) would induce larger and unpredictable frictional forces, especially for softer materials like polymers. It is also shown by Pandit and Srinivasan (2017) that for the cases when the deflection is comparable to the roller size, the displacement of the contact point must be considered. In their work, they showed that an increasing roller radius can have a non-negligible stiffening effect.

Ministry of Science and Higher Education
Republic of Poland

The publication has been funded by the Polish Ministry of Science and Higher Education under the Excellent Science II programme "Support for scientific conferences".
The content of this article was presented during the 40th Danubia-Adria Symposium on Advances in Experimental Mechanics, Gdańsk, Poland, September 24–27, 2024.

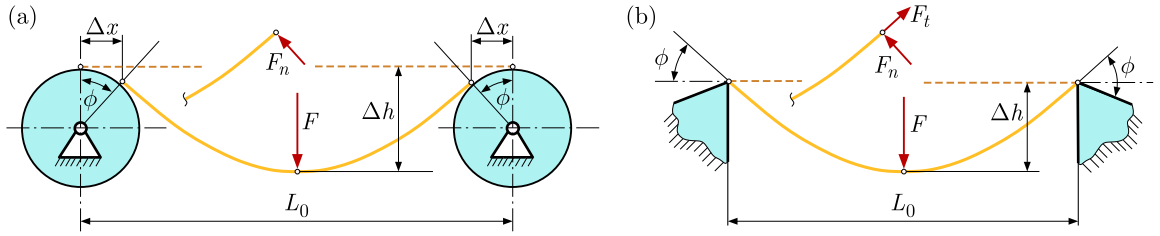

Fig. 1. Three-point bending support solutions: (a) rollers on bearings; (b) simple edge supports.

In this manuscript, a novel support type is proposed, which functions as a frictionless edge. It not only eliminates friction between the support and the specimen, but also fixes the point of contact, which can make the mechanical modeling easier, as it eliminates a source of nonlinearity. Furthermore, as later presented, one can choose theoretically any supporting pin diameter, which may be used to reduce contact pressure, if needed.

2. Experimental device

The schematic drawing of the support is presented in Fig. 2. The specimen (A) is sitting on a rolling axle (B), which is supported on both ends by deep-groove ball bearings (C). The bearings can freely roll on a cylindrical surface (D) that is machined into an aluminum supporting block (E). The supporting block (E) is milled in such a way that the specimen ends may undergo rotations up to 90°. The cylindrical surface on which the bearings roll should have a diameter that is twice the diameter of the bearings (C) and the axle (B) as follows:

$$D = d + d_b. \tag{2.1}$$

With this setup (if one neglects the weight of the axle and bearings), the beam (A) will always push the axle (B) in a position where the contact forces go through the center of the cylinder (D) and axle (B). This, together with Eq. (2.1) implies that the contact point must always coincide with the center point. The bearings (C) ensure that the frictional forces remain negligible.

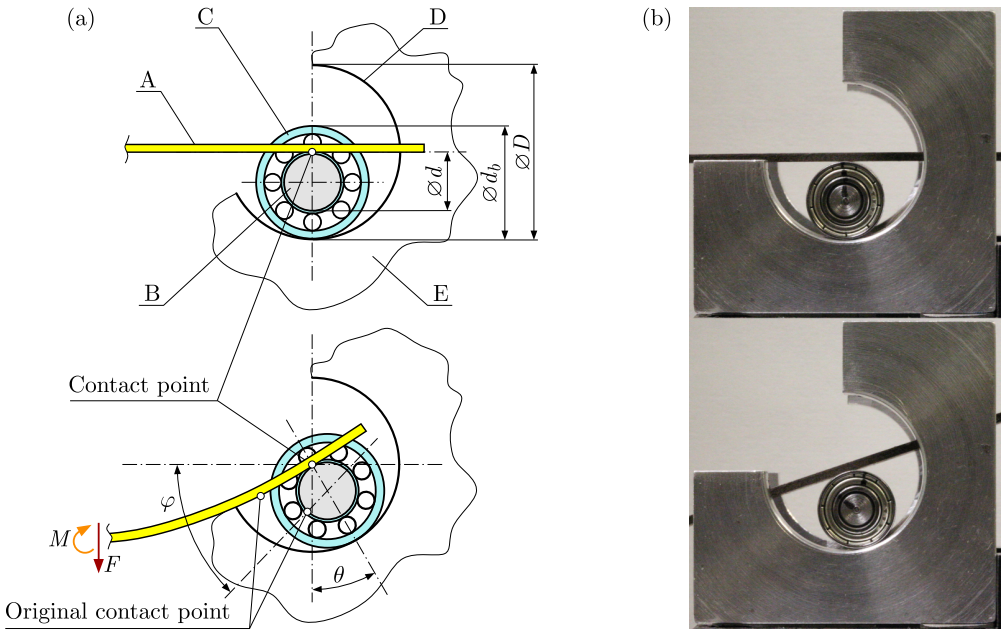

Fig. 2. Proposed solution and the working principle of a frictionless edge support (a), and the realized support during a measurement (b).

A demonstration of the support during a measurement is presented in Fig. 2b in a loaded and in an unloaded state.

For a better visibility of the beam during the loading process, one can equate the bearing and axle diameters. Thus:

$$d = d_b = \frac{D}{2}. \tag{2.2}$$

While theoretically the contact point always coincides with the center of the circular track, with the gravitational force acting on the rollers this is not always the case. For a deeper insight into the behavior of the support, the reader is referred to Fig. 3, which shows the free-body diagram of the roller.

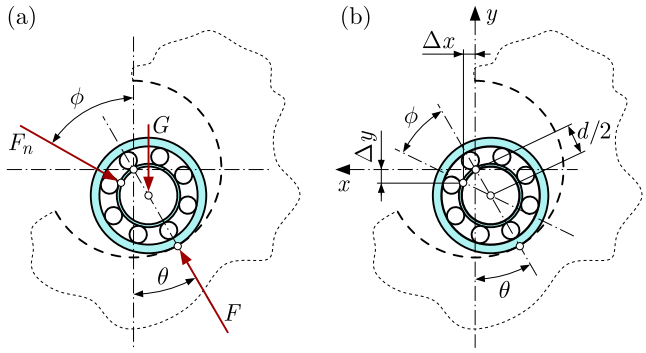

Fig. 3. Free-body diagram of the roller with gravitational force (a), and the important dimension parameters (b).

Solving the equilibrium of three forces yields the contact angle θ and contact force F as functions of the normal force on the beam (F_n) and the beam end's tangent angle (ϕ) as follows:

$$\theta = \operatorname{acot}\left(\cot\phi + \frac{G}{F_n \sin\phi}\right), \qquad F = \sqrt{F_n^2 + G^2 + 2\,G\,F_n\cos\phi}. \tag{2.3}$$

Given the nature of the cotangent function and the fact that both G and F_n are positive numbers, the contact angle θ will always "fall behind" the beam end's rotation angle. The angular difference results in a shifted contact point, as presented in Fig. 3. The contact point's displacement can be given for the x- and y-directions as the following:

$$\Delta x = \frac{d}{2}\left(\sin\phi - \sin\theta\right), \qquad \Delta y = \frac{d}{2}\left(\cos\phi - \cos\theta\right). \tag{2.4}$$

For any F_n and θ combination, the contact angle and the contact point displacement can be calculated. However, the latter changes the beam length that undergoes bending, which in return changes the $F_n\phi$ pair in the equilibrium state. The equilibrium for a given F_n normal force can be obtained iteratively. For a given F_n value, the iteration goes as follows: start by assuming that the support points are at their nominal locations (at a distance of L_0) and find the rotation of the beam end. For the beam end rotation ϕ_i, find the contact angle θ_i and the expected contact point displacement in the x direction (Δx_i) by using Eqs. $(2.3)_1$ and $(2.4)_1$. Based on the Δx estimate, update the support span by setting $L_{i+1} := L_i - \Delta x_i$, and solve the beam equilibrium for the new support span, with the same F_n shear force on the beam end. In the simulations, a convergence criterion of $|\Delta x_i - \Delta x_{i-1}| < 10^{-5}$ mm was used. In our experience, this iteration converges in 4–5 steps. These calculations were repeated for several shear force values to obtain the behavior of the beam in a nonlinear three-point flexural test with the frictionless edge supports. The shape of the elastica curve was found by using a numerical method developed earlier for numerical simulation of the three-roll bending process (Máté & Szekrényes, 2020).

3. Measurement and proof of concept

A modular three-point bending device was manufactured at the Applied Mechanics Department of the Budapest University of Technology, which can be operated by any suitable tensile testing machine. This device can be configured for three- and four-point bending tests, and it can incorporate the above-mentioned support type. During the tests, an Instron 3345 universal testing machine was used. The former was used while capturing the movement of the bearings and the shafts, simply because there was enough space for the camera setup (as presented later, the movement of the bearings is obtained from photographs via simple DIC algorithms similar to the algorithm developed by Sutton *et al.* (1983).

In the manufactured version of the support, the axle had a diameter of $d = 13\,\text{mm}$ (with $D = 26\,\text{mm}$), and the bearings were of type 618 (Koyo Jtekt, 2024). The bearings and the shaft have the same diameter, as it can also be seen in Fig. 2. It is emphasized here that the beam's centerline actually rolls on a virtual roller of radius $R_1 = t/2$ (where t is the specimen thickness) if the shaft perimeter touches the track's center point. In our setup, this was the case. However, one can design supports with a modified Eq. (2.1), which includes the specimen thickness and reduces the radius of the virtual roller to zero:

$$D = d_b + d + t. \tag{3.1}$$

The weight of the axle-bearing assembly plays a crucial role in the contact point's displacement. A reduced weight of the shaft helps in reducing the contact point displacement. The manufactured shaft, together with the bearings, weighs 48.7 g. Thus, $G = 0.478\,\text{N}$.

The measurement setup was tested on two slender composite beams and a thin steel strip. The data for these specimens and the measurement setup is given in Table 1.

Table 1. Specimen and three-point bending test data.

Specimen	b [mm]	t [mm]	L_0 [mm]	Material	Flexural modulus of elasticity [GPa]
Composite 1	25.1	1.22	148.2	8-ply Hexply M92 55 % 220	13.81
Composite 2	25.2	2.43	148.2	16-ply Hexply M92 55 % 220	14.02
Steel	30.15	1.54	301	Spring-grade steel	200.00

All three specimen types listed in Table 1 were tested both on the novel frictionless edge support and on simple, smoothed edge supports. The measurement setup is shown with the Composite 1 specimen under testing in Fig. 4. In the first two photographs, the measurement can be seen with the frictionless edge support mounted on the testing jig. The third photograph shows the simple edge realized by two 8 mm thick steel blocks mounted instead of the new support type. Before measurement, the laser cut edge was deburred with sandpaper in order not to cut into the beam, especially in the case of the composite specimens.

The measurement results were compared to the simulation results obtained by the iterative solution presented in Section 2, based on (Máté & Szekrényes, 2020). The measurement results for the displacement-force characteristics for the three specimens are presented in Fig. 5. In the plot legends, "F.E." stands for "frictionless edge support", while "S.E." stands for "simple edge support". It is important to emphasize that the simulation results here are for the actual setup, where the shaft and bearing assembly has weight. The beam's own weight was considered negligible.

The composite beam's flexural modulus of elasticity was measured with classical three-point flexural tests, and in the simulations these beams were treated as if they were made of linear, isotropic materials. As can be seen in Fig. 5, the thicker composite beam's hysteretic behavior cannot be neglected anymore, as it undergoes relatively large deformations. To ensure that the

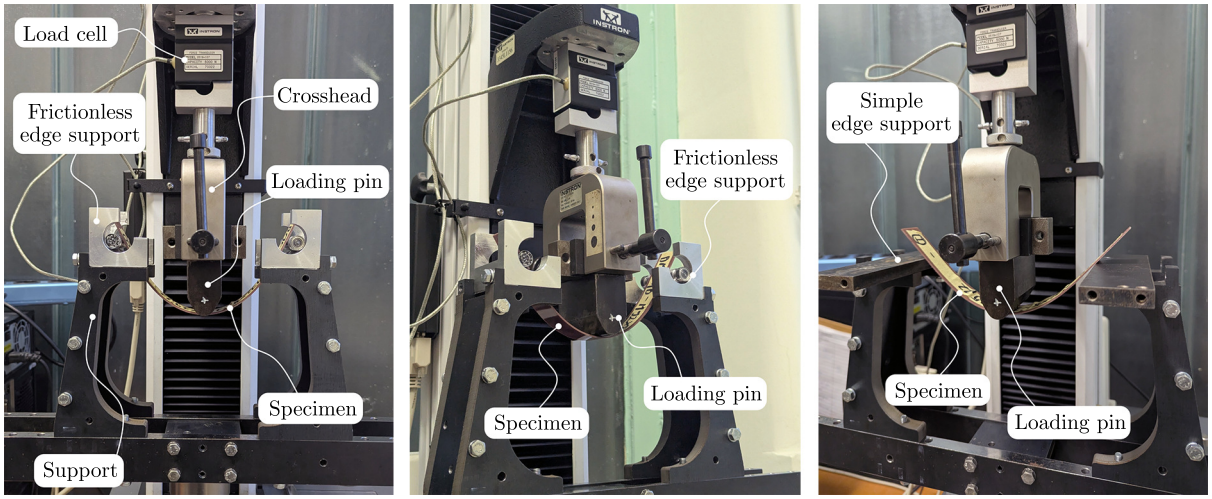

Fig. 4. Measurement setup shown with the frictionless edge support (left and middle) and with the simple edge support (right).

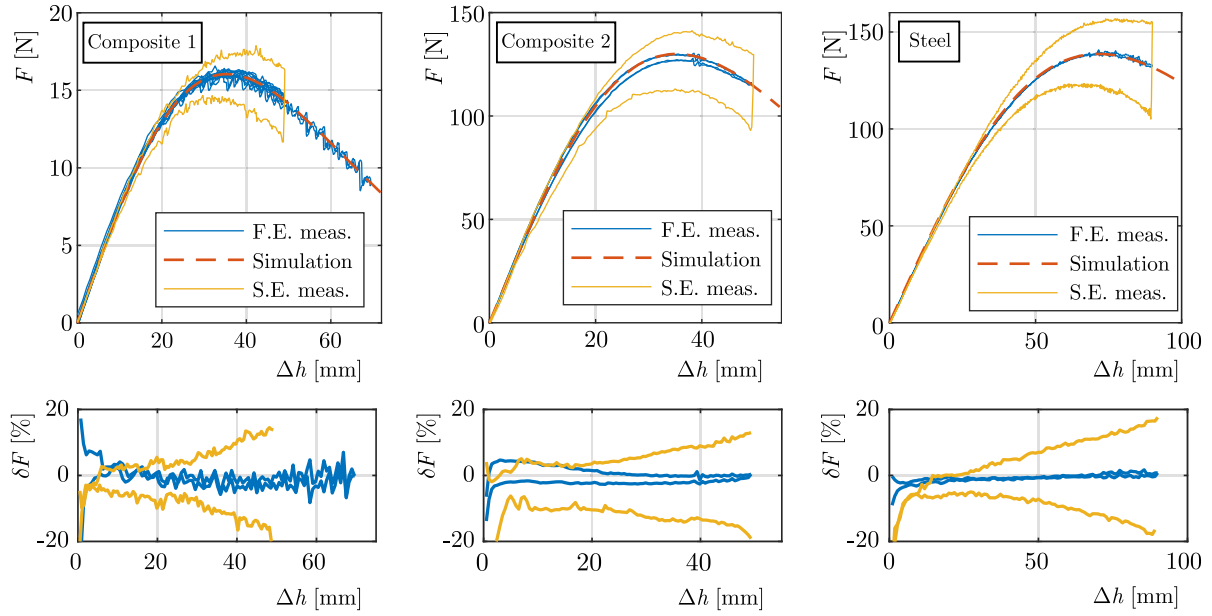

Fig. 5. Comparison of the measured and simulated deflection-force characteristics for the three specimens (upper row), along with the relative difference of the measurements to the simulations (lower row).

measurements were conducted in the elastic region, both the loading and unloading cycles are shown in the figures. To show that the hysteresis that can be seen in the measurements made with the simple edge support is not caused by the beam material or the bearing friction, a total of six load cycles are plotted in Fig. 5 for the Composite 1 specimen in the case of measurements made with the simple edge support. These consist of five shorter (50 mm displacement) and a longer cycle (70 mm displacement). The composite beam follows the same path each time it is cycled, showing that the material hysteresis and the bearing friction are negligible. In the case of the steel beam, the match between the simulation and the measurements is remarkable. The repeatability of the measurement was exceptional for all specimen types. The lower row of Fig. 5 shows the relative difference of the measured force to the simulation in percentage as a function of the displacement Δh.

It is also important to examine the deviation of the realistic loading characteristics (which consider the shaft weight) from the ideal ones (with stationary contact point, i.e. simulation results with $G = 0\,\mathrm{N}$). To quantify the imperfection of the frictionless edge support, the sim-

ulations, also visible in Fig. 5, were conducted for the weightless, ideal case too. The relative difference is given in Fig. 6 as

$$\delta F(\Delta h) = 100 \left(\frac{F^r(\Delta h)}{F^i(\Delta h)} - 1 \right), \tag{3.2}$$

where $F^r(\Delta h)$ denotes the loading characteristic obtained from simulations which consider the shaft's weight (also plotted in Fig. 5), while $F^i(\Delta h)$ stands for the results of the ideal case (i.e. simulation result with stationary contact point). As Fig. 6 shows, the imperfection in the loading characteristic of the new support type caused by the roller weight can be considered negligible if the test specimen is stiff enough. For example, there is almost an order of magnitude difference between the two composite specimens, only because of the difference in bending stiffness (similar support span). The oscillatory characteristic of the relative difference functions in Fig. 6 is caused both by the inaccuracies of the numerical simulations and the fact that the resulting $F^r(\Delta h)$ and $F^i(\Delta h)$ functions were resampled using a cubic spline interpolation to get their value at the same Δh locations. The theoretical contact point displacement can also be extracted from the simulations. The Δx and Δy values as functions of deflection Δh for the three specimens are displayed in Fig. 7.

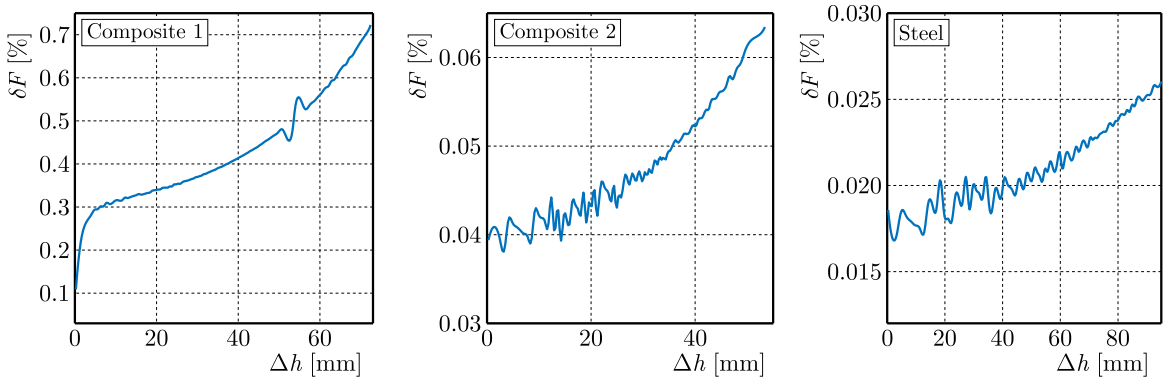

Fig. 6. Relative error of the "measured" force F, when gravity acts on the roller assembly, compared to the ideal case, with weightless rollers.

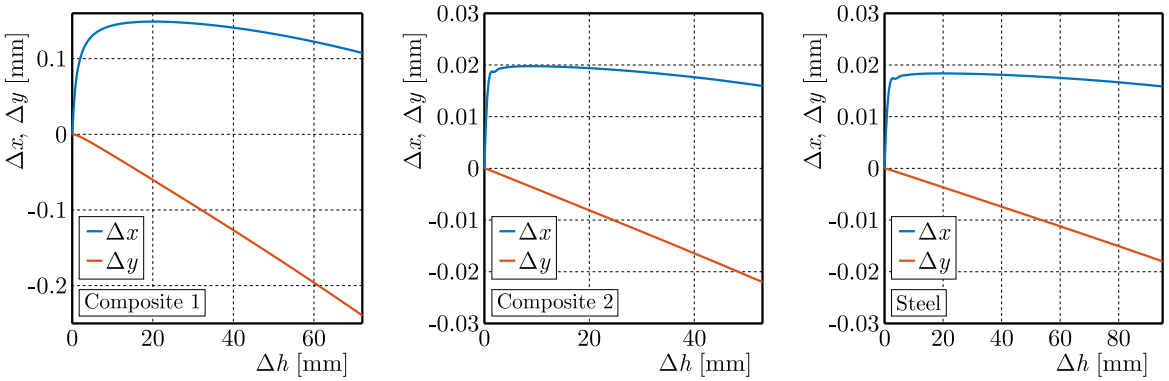

Fig. 7. Expected, theoretical displacement of the contact point for the three specimen types.

As Fig. 7 shows, the displacement of the contact point is expected to be very small, even for the Composite 1 specimen with the lowest flexural rigidity. These values can be lowered further either by using either a smaller shaft diameter, according to Eq. (2.4), or by reducing the rolling element's weight. Note that the simulation results in Fig. 7 are the contact point displacements compared to a simple edge support with zero radius, and do not consider the fact that the centerline of the beam rolls on a virtual roller with a radius of $t/2$. However, if needed,

unique designs may be created based on Eq. (3.1) for given specimen thicknesses, which ensure that the support of the centerline becomes stationary.

To compare the shape of the simulated elastica curve and the measurements, the testing jig was transferred to an Alfred J. Amsler & Co. tensile testing machine so that photographs could have been taken from a proper distance. This ensures that the central projection of the camera gets as close as possible to the parallel projection, making the photograph suitable for accurate measurements. Then, the elastica curve was calculated for the measured deflection and plotted onto the photograph, as shown in Fig. 8.

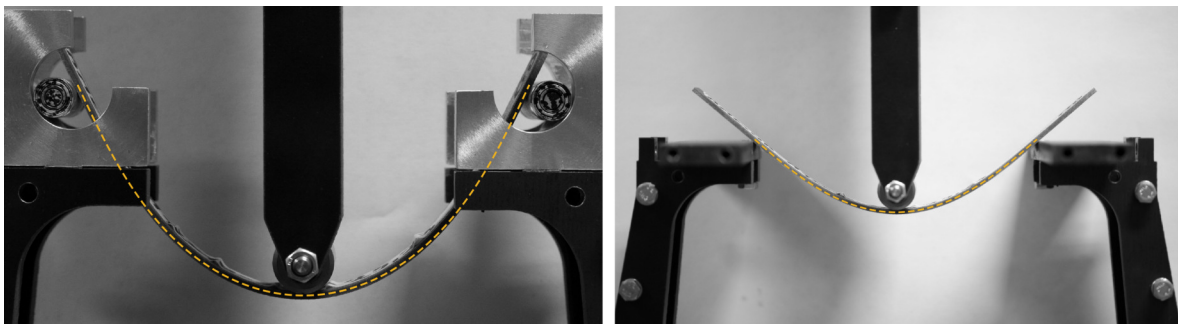

Fig. 8. Comparison of the elastica curve (dashed yellow line) with the actual measurement of a composite beam both on the frictionless edge (left) and the simple edge (right).

This was done for the Composite 2 specimen. The images in Fig. 8 were taken at $\Delta h = 68\,\mathrm{mm}$ with the frictionless edge, and at $\Delta h = 37\,\mathrm{mm}$ with the simple edge support. The simulated results (simulation was done without considering friction) represented by the dashed curve match remarkably well with the curve on the photograph. While some deviation can be observed between the elastica curve and the deformed shape of the beam when using simple edge supports, this difference is hardly noticeable.

4. Measurement of the shaft and bearing rotation

The previously presented setup was used for a further analysis of the supports. An investigation was led on whether slip occurs in the system, by capturing the rotation of the shafts and the bearings on the camera. Several photographs were taken during a full load cycle about the supports (also shown in Fig. 9) at 21 load levels. The black random pattern on the axle and the bearing seen in Fig. 9 is there to show the rotation of the shaft and bearing outer ring.

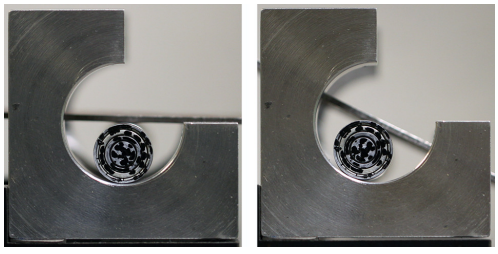

Fig. 9. Pattern on the roller assembly used to track the rotation of the shaft and bearing outer ring.

The rotational angle of the shaft and outer ring (φ and θ in Fig. 2) was traced with the help of a custom MATLAB Digital Image Correlation algorithm. The displacement of the loading pin was determined based also on digital image processing. The measured rotations are given in the left side of Fig. 10, for the Composite 2 test specimen. Here, the yellow continuous curve shows the theoretical outer ring rotation θ (calculated with weightless rollers). The measurements show that, as expected, the outer ring rotation θ is smaller than the rotation in the ideal, weightless

case. The discrete data contains a full load cycle. To check whether there is a slip in the system, one can calculate the increment in the beam specimen's working length (arc-length between the two contact points with the supports). The arc-length increment between the contact point with the rollers can be given as a function of the rotation angles as

$$\Delta L = \frac{d+t}{2}(\varphi_l + \varphi_r - \theta_l - \theta_r), \tag{4.1}$$

where the subindices "l" and "r" refer to the left and the right side, respectively. In the right side of Fig. 10 the expected theoretical increment is plotted together with the increment calculated with Eq. (4.1), based on the measured angle values, also presented in the left part of Fig. 10. The figure also shows the relative difference between the measurements and the theoretical calculations in the bottom plots. These show that the errors present in the beginning fade away with increasing displacement Δh. The bottom left plot of Fig. 10 also shows that the two supports behaved identically during the measurements.

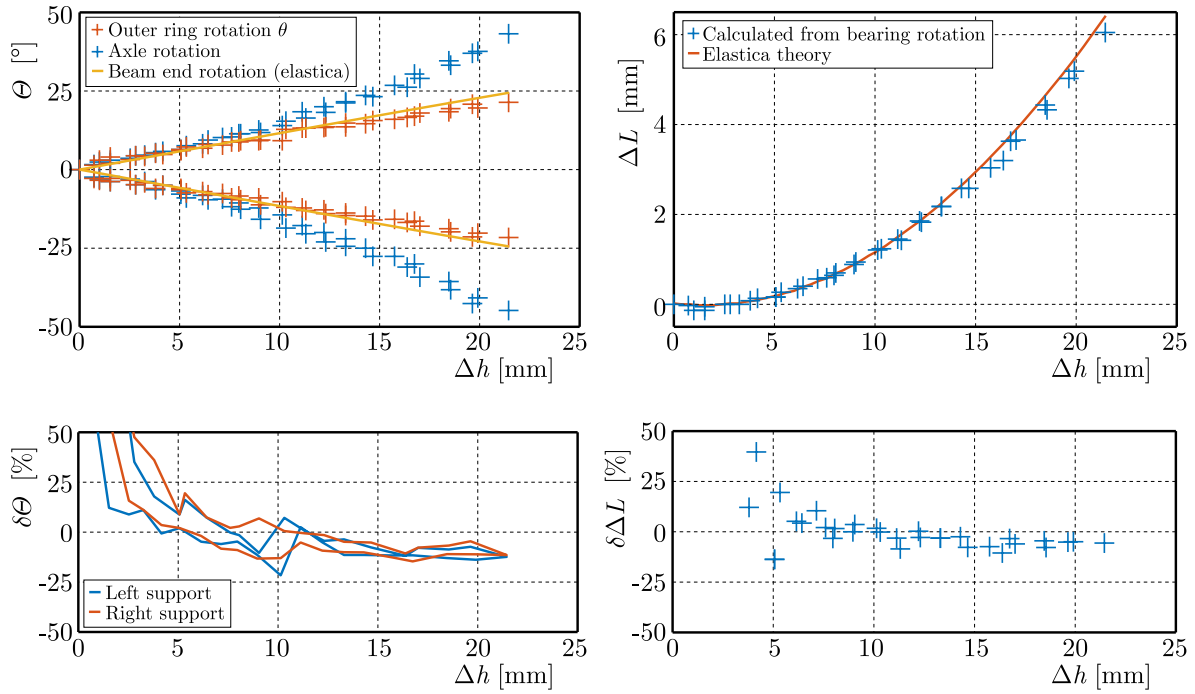

Fig. 10. Rotation of the axle and outer ring (left), and the working beam length increment calculated from the measured bearing and axle rotations (right), along with relative difference of the measurements compared to calculations from the elastica theory, shown in the bottom plots.

5. Conclusions

In this paper, a novel support is proposed, which can simulate a frictionless edge in the case of the three- and four-point bending tests. The mechanical analysis of the support was performed, and a support prototype was manufactured. Multiple tests conducted on several steel and composite beam specimens proved that the concept functions as expected, with negligible friction and contact point displacement. In the theoretical analysis, the bearing friction was neglected, but the effect of the roller's weight was considered. The measurement results revealed that the bearing friction is truly negligible, and that the supports function perfectly, as expected, without a significant contact point displacement. We compared the force-displacement load characteristics obtained from simulations with measurement results. The results were in exceptional agreement with the numerical calculations. We also measured the shaft and bearing rotation by using our simple DIC algorithm, on whose basis the arc-length increment was calculated.

The arc-length increment also follows the theoretical prediction and shows negligible hysteresis, meaning that there is no significant slip between the rollers, the beam, and the track.

Acknowledgments

This work has been supported by the National Research, Development and Innovation Office (NRDI) under grant no. 134303. The research reported in this paper has been supported by project no. TKP-6-6/PALY-2021 provided by the Ministry of Culture and Innovation of Hungary from the National Research, Development and Innovation Fund, financed under the TKP2021-NVA funding scheme.

We would also like to thank Aurél Horváth and the BME Suborbitals competition team for providing the composite beam specimens.

References

1. Arnautov, A.K. (2005). The method of three-point bending in testing thin high-strength reinforced plastics at large deflections. *Mechanics of Composite Materials*, *41*(5), 467–476. https://doi.org/10.1007/s11029-005-0072-2
2. Batista, M. (2015). Large deflections of a beam subject to three-point bending. *International Journal of Non-Linear Mechanics*, *69*, 84–92. https://doi.org/10.1016/j.ijnonlinmec.2014.11.024
3. Koyo Jtekt, Ball & Roller Bearing catalog. Retrieved December 15, 2024, from https://koyo.jtekt.co.jp/en/support/catalog-download/
4. Máté, P., & Szekrényes, A. (2020). Numerical modelling of the three-roll bending process of a thin plate. *Műszaki Tudományos Közlemények*, *13*, 133–136. https://doi.org/10.33894/mtk-2020.13.24
5. Mujika, F. (2006). On the difference between flexural moduli obtained by three-point and four-point bending tests. *Polymer Testing*, *25*(2), 214–220. https://doi.org/10.1016/j.polymertesting.2005.10.006
6. Pandit, D., & Srinivasan, S.M. (2017). Large elasto-plastic deflection of thin beams with roller support contact. *Procedia Engineering*, *173*, 1079–1084. https://doi.org/10.1016/j.proeng.2016.12.188
7. Sutton, M.A., Wolters, W.J., Peters, W.H., Ranson, W.F., & McNeill, S.R. (1983). Determination of displacements using an improved digital correlation method. *Image and Vision Computing*, *1*(3), 133–139. https://doi.org/10.1016/0262-8856(83)90064-1
8. West, D.C. (1964). Flexure testing of plastics. *Experimental Mechanics*, *4*(7), 185–190. https://doi.org/10.1007/BF02323649

Manuscript received December 16, 2024; accepted for publication April 24, 2025; published online July 26, 2025